J. Fluid Mech. (1995), *vol.* 286, *pp.* 25–48

Marangoni effects of adsorption–desorption controlled surfactants on the leading end of an infinitely long bubble in a capillary

By K. J. STEBE[1] AND D. BARTHÈS-BIESEL[2]

[1] Department of Chemical Engineering, The Johns Hopkins University, Baltimore, MD 21218, USA

[2] Université de Technologie de Compiègne URA 858, BP 649, 60206 Compiègne Cedex, France

(Received 29 July 1993 and in revised form 26 June 1994)

The leading end of an infinitely long gas bubble which displaces a viscous surfactant solution in a capillary tube is studied. The surfactant is present at elevated concentration and has sorption controlled mass transfer. The displaced fluid wets the wall, forming a continuous liquid film between the bubble and the capillary wall. Both the thickness of this film and the additional pressure required to aspirate the bubble depend upon the Marangoni stresses caused by non-uniform surfactant adsorption along the interface. The equations governing this flow are solved at asymptotically small capillary number for the case where the balances of momentum and mass transfer are coupled to leading order. As the Marangoni effect is increased over several orders of magnitude, the additional pressure and the wetting-layer thickness increase above the stress-free interface values found by Bretherton (1961) and approach an upper bound of $4^{2/3}$ times the Bretherton values. Accompanying changes in the surface tension, Marangoni stress and surface velocity profiles as this upper bound is approached are described. Finally, surface viscosities that are intrinsic to the interfacial region are incorporated in the analysis. When small departures from surface equilibrium states are considered, the terms representing surface viscous effects have the same functional form as the Marangoni stresses and result in thicker films and higher additional pressures.

1. Introduction

The motion of a long gas bubble which displaces a viscous liquid in a capillary tube has been studied extensively to understand the flow of immiscible fluids in porous media. It is well established that the presence of surface-active agents may affect the hydrodynamics of such flows considerably. In many situations of practical interest, surfactants are present at elevated concentrations (e.g. foam mobility control in tertiary oil recovery, and in the human micro-circulation when gas bubbles appear) and experimental results differ significantly from predictions based on clean surface conditions. When the displaced fluid wets the wall, there is a continuous liquid film between the bubble and the tube wall. The two quantities of interest that can be measured and computed are the film thickness h'_∞ and the additional pressure drop $\Delta p'$ created by the presence of the bubble. We propose here an asymptotic study of these quantities in the case where the surfactant mass transfer is adsorption–desorption controlled.

A thorough review of the previous work on this flow is given in both the recent

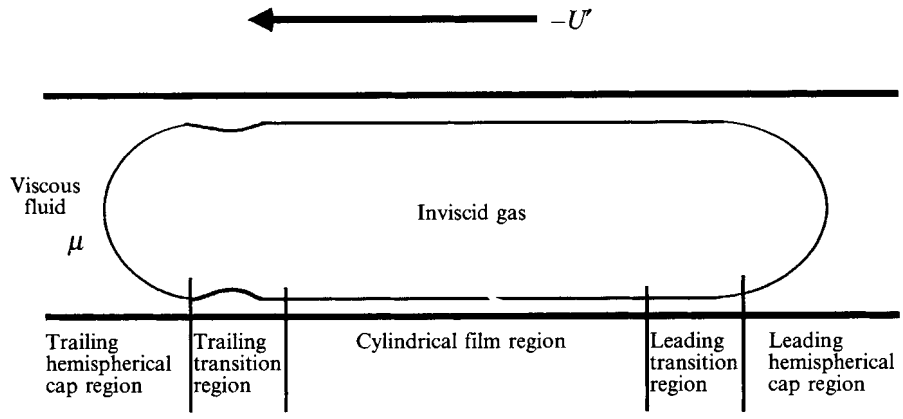

FIGURE 1. The five regions in the flow of an infinitely long bubble drawn at asymptotically small capillary number are shown in a bubble fixed reference frame.

articles of Ratulowski & Chang (1990) and of Stebe, Lin & Maldarelli (1991). Therefore, we recapitulate the literature only briefly here.

In the case in which no surfactant is present, Bretherton (1961) studied the motion of a long gas slug moving in a liquid-filled capillary tube. Then, at low Reynolds number, and in the absence of gravitational effects, the flow depends solely on the capillary number Ca, a ratio of viscous to surface tension forces

$$Ca = \mu' U'/\sigma',$$

where μ' is the viscosity of the displaced phase, U' is the velocity at which the gas bubble is drawn through the tube and σ' is the interfacial tension of the gas–liquid interface.

For asymptotically small Ca, the gas slug can be divided into five regions (figure 1). At either end of the bubble are hemispherical regions, where capillary forces alone determine the interfacial shape and pressure. The hemispheres are joined via transition regions at either end of the bubble to the long cylindrical region. Bretherton established analytically that the thickness of the uniform wetting layer in the cylindrical region, h'_∞, is determined by the leading end of the bubble, and that the additional pressure drop does not depend on the bubble length. Both quantities are proportional to $Ca^{2/3}$, and are found to have the values:

$$h'_\infty/R' = 1.34\, Ca^{2/3}, \quad \Delta p' R'/\sigma' = 9.40\, Ca^{2/3},$$

where R' is the tube radius. The Bretherton analysis has been extended to Hele-Shaw cells, and expanded in its range of validity by Park & Homsy (1984).

Many experiments have been performed in an effort to confirm these analytical clean interface results. In all of the 'surfactant free' studies (in which trace surface active contaminants were probably present) wetting-layer thicknesses in excess of those predicted by this asymptotic analysis are systematically reported (see e.g. Bretherton 1961; Chen 1985; Schwartz, Princen & Kiss 1986). Furthermore, these discrepancies worsen with decreasing capillary number, counter to expectations for a small Ca analysis.

Additional pressure drop measurements across a gas slug have also been found to be consistently in excess of those predicted by Bretherton's theory, and to depend upon the bubble dimensions. Specifically, in the case of a gas slug being drawn through a capillary filled with an electrolytic solution, Marchessault & Mason (1960) report a

pressure drop that is proportional to slug length for moderately long bubbles. While the authors did not add surfactant to their solution, it is likely that surface active impurities were present. Similar behaviour has been observed when surfactant is deliberately present. For example, when sodium dodecyl sulphate (SDS) is added to saline at elevated concentrations, Barthès-Biesel, Moulai-Mostefa & Meister (1986) find a pressure which first increases with bubble length and then asymptotes to some constant value significantly in excess of the clean surface theory of Bretherton. Additional experimental evidence of elevated pressure drops in the presence of surfactant adsorption is provided by Hirasaki & Lawson (1986), who added sodium dodecyl benzene sulphonate to water, as well as by Ginley & Radke (1989) who measured the pressure needed to displace gas bubbles in capillaries filled with solutions of SDS in a mixture of glycerol and water. These experimental studies establish that surfactant adsorption can create stresses which resist the motion of long gas slugs in capillaries. As a result of these stresses, higher driving pressures are required to aspirate the long gas slugs, and thicker wetting layers are formed than those predicted for clean surface conditions.

As explained by Levich (1962), surfactant molecules adsorb along fluid interfaces, where they lower the interfacial tension. Convection tends to increase (decrease) the surface concentration of adsorbed surfactant near stagnation zones where the flow converges (diverges). However, both adsorptive–desorptive and bulk diffusive fluxes tend to diminish gradients in surface concentration. If either of these fluxes is slow, a non-uniform distribution of adsorbed surfactant is established, causing a gradient in the interfacial tension, and thus a Marangoni stress. This stress, exerted by the interface on the fluid, is directed from regions of lower surface tension toward regions of higher tension.

In a bubble fixed reference frame, the capillary wall moves with velocity $-U'$, and the fluid far from the bubble is in Poiseuille flow with a positive centreline velocity. Consequently, there is a stagnation ring at either end of the bubble, as well as a stagnation point at either pole. Therefore, as shown in figure 2, surfactant accumulation with a concomitant decrease in surface tension is expected at the leading pole, while surfactant depletion with an accompanying elevation in surface tension is anticipated at the leading stagnation ring.

Several theoretical studies have been undertaken to understand the effect of surfactants in capillary slug flows. Thus far, all of these studies involve perturbations from either clean interface or equilibrium states for a long bubble moving at asymptotically small Ca. For infinitely long bubbles in these asymptotic regimes, both Herbolzheimer (1987) and Chang & Ratulowski (1987) show that the surfactant effect reaches a maximum. In this limit, the equations of mass transfer and fluid mechanics are decoupled in the transition region. The values of both the leading-end additional pressure and wetting-layer thickness for this maximum effect are simply $4^{2/3}$ times the Bretherton expressions. This limit bounds the data for ostensibly clean flows appearing in the literature. In addition, at elevated surfactant concentrations, the maximum surfactant effect bounds the pressure data to which long bubbles asymptote in the study of Barthès-Biesel *et al.*

Recently, the influence of trace adsorption of bulk insoluble surfactants on the motion of long drops or bubbles has been studied by Park (1991) and by Borhan & Mao (1992). In this regime the surfactant distribution is determined by the competition between surface convective and surface diffusive fluxes. Park integrated the equations for the dip-coating of a plate, which are the same as those that govern the front end of an infinitely long bubble. Uniform wetting-layer thicknesses in excess of the

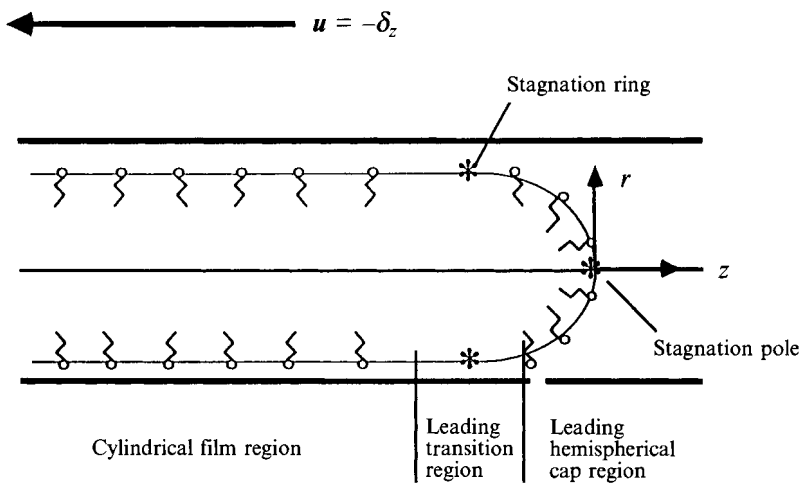

FIGURE 2. The surfactant distribution at the leading edge of the bubble is shown. Surface convection tends to accumulate surfactant at the leading stagnation pole, and to deplete the surface concentration near the leading stagnation ring. The cylindrical polar coordinate system (r, z) is also shown.

Bretherton value are found, which are bounded above by the maximum surfactant effect value. The effects of insoluble surfactant on droplets of finite length at low *Ca* have been investigated by Borhan & Mao who use the boundary integral technique to integrate Stokes' equations for a viscosity ratio of 1.0 and for lengths of up to five times the tube radius. For these moderately long drops the pressure required to aspirate the flow increases as the surface diffusion rate decreases.

The distribution of bulk soluble surfactant depends strongly on the transport of surface active molecules from the bulk phase to the interface. There are two main transport processes: transport from the bulk to the fluid sublayer by bulk diffusion and convection, followed by exchange between the sublayer and the interface by adsorption and desorption.

When only trace contaminants are present (as in the apparently clean systems) bulk mass transfer is important, and the surface concentration of adsorbed surfactant is small. The leading end of an infinitely long bubble has been studied extensively in this limit by Ratulowski & Chang who derive the equations for various convective, diffusive and sorptive kinetic timescales. They integrate a convection-equilibrium model, in which convection determines the bulk surfactant concentration profile. The kinetics of adsorption and desorption are assumed to be instantaneous, so that local equilibrium between the interface and the sublayer is maintained. They also integrate a diffusive–adsorption model, where both bulk diffusion and adsorptive–desorptive exchange determine the surfactant distribution. For both models, the pressure and wetting-layer thickness are bounded below by the Bretherton clean surface limit and approach the maximum surfactant effect as the surface elasticity (a measure of the dependence of surface tension on surfactant adsorption) becomes large. The effects of diffusion controlled mass transfer on a long bubble of finite length has been studied by Park (1992) who finds that the presence of a stagnated region causes pressure drops that depend upon bubble length.

The other situation of interest is encountered when the bulk concentration is high enough to neglect bulk diffusion, and the rate of adsorptive–desorptive exchange governs the flux of surfactant to the interface. In this regime, the surface concentration deviates only slightly from the value corresponding to thermodynamic equilibrium

with the bulk. Hirasaki & Lawson derived the governing equations of a gas slug for the case where the Marangoni effect is coupled with the hydrodynamics to leading order. Rather than integrating these equations, they require that the film thickness remain constant throughout the transition region, and determine h'_∞ empirically. Barthès-Biesel *et al.* integrate these film equations in the vicinity of the back stagnation ring, and find an elevated additional pressure drop that depends on bubble length in a fashion qualitatively similar to the experimental data. Finally, Ginley & Radke derive and solve the equations for the leading end of the bubble for the case in which the sorption kinetics and fluid mechanics are weakly coupled, so that, to leading order, the flow is governed by Bretherton's equations. In the limit of fast adsorption–desorption kinetics, they find a positive first-order correction to the Bretherton pressure. Their film thickness, however, decreases to first order. This is unexpected, since all of the wetting-layer thickness measurements reported in the literature are larger than those reported by Bretherton.

In conclusion, Marangoni effects on the flow of long gas slugs are well understood in the case of trace surfactant adsorption. Such is not the case for surfactants present at elevated bulk concentration. The objective of this paper is to consider the case where the surfactant flux is adsorption–desorption controlled and the equations of momentum and mass transfer are coupled to leading order. The effects on this flow of surface viscosities are also discussed.

A dimensional analysis of the equations of mass and momentum transfer is presented in the next section, along with a thorough discussion of the dimensionless groups that appear in the literature. In §3, following Bretherton, the equations are rescaled appropriately for the different regions and the ordering of the dimensionless groups for which this analysis is valid is specified. In §4, the equations and matching conditions governing the film thickness and the pressure drop in the sorption controlled limit are derived and their numerical integration is described. Finally, the results of the integration and matching are discussed in §5.

2. Governing equations

An infinitely long, inviscid gas bubble is drawn slowly with velocity U' through a capillary tube of radius R' filled with an incompressible Newtonian fluid of viscosity μ'. The flow geometry is shown in figure 2 in the bubble fixed reference frame. As the bubble advances, a thin wetting layer of constant thickness h'_∞ is established in the cylindrical region, far behind the leading edge of the bubble. The gas phase pressure remains uniform at some reference pressure, arbitrarily taken here to be zero.

A surfactant is dissolved in the liquid phase. In the absence of flow, the surfactant has a bulk concentration C'_{eq}, to which corresponds a surface concentration Γ'_{eq} and an interfacial tension σ'_{eq}.

All dimensional quantities are denoted with a prime, while dimensionless quantities are unprimed. Throughout the literature, the following scales are adopted to put the governing equations into dimensionless form: R' for lengths, U' for velocities, and $\mu' U'/R'$ for viscous stresses. However, for the surfactant related quantities, different scales have been used, depending upon whether small departures from equilibrium or a clean surface state are considered. Since this study focuses on elevated surfactant concentrations, perturbations from an equilibrium surfactant distribution are considered, and surface concentration, surface tension and bulk concentration are scaled with their equilibrium values, Γ'_{eq}, σ'_{eq} and C'_{eq}, respectively. For this choice of characteristic surface tension, pressure scales as σ'_{eq}/R'.

2.1. *Hydrodynamics*

The capillary radius is assumed to be small enough that gravity can be neglected and the flow is axisymmetric. The system is described using a cylindrical polar coordinate system (r, z) as shown in figure 2 with the origin located at the leading pole, and the z-axis pointing into the viscous phase.

Assuming that the Reynolds number for this flow,

$$Re = \rho' U' R'/\mu',$$

is small, the steady state flow field of the viscous fluid is governed by Stokes' equations:

$$Ca\nabla^2 \boldsymbol{u} = \nabla p, \tag{2.1}$$

$$\nabla \cdot \boldsymbol{u} = 0, \tag{2.2}$$

where $\boldsymbol{u}$ is the velocity field and p is the hydrodynamic pressure in the liquid phase. The capillary number, Ca:

$$Ca = \mu' U'/\sigma'_{eq},$$

is based on the equilibrium surface tension.

Far ahead of the bubble, the liquid is in Poiseuille flow:

$$\lim_{z\to\infty} u_z = \frac{1}{4Ca}\frac{\mathrm{d}p}{\mathrm{d}z}\bigg|_{z\to\infty}(1-r^2)-1. \tag{2.3}$$

The no-slip condition at the capillary wall requires:

$$\boldsymbol{u} = -\boldsymbol{\delta}_z \quad \text{at} \quad r = 1, \tag{2.4}$$

where $\boldsymbol{\delta}_i$ is the unit coordinate vector in the ith direction. Boundary conditions on the velocity and pressure field are imposed along the interface, the position of which is an unknown, defined by:

$$r = H(z),$$

with unit tangent and normal vectors $\boldsymbol{t}$ and $\boldsymbol{n}$ (directed into the viscous phase). The surface gradient operator, ∇_s is defined as:

$$\nabla_s = (\boldsymbol{I} - \boldsymbol{nn})\cdot\nabla,$$

where $\boldsymbol{I}$ is the identity tensor and $\boldsymbol{nn}$ is a dyadic product.

The kinematic condition at the interface is:

$$\boldsymbol{n}\cdot\boldsymbol{u} = 0 \quad \text{at} \quad r = H(z). \tag{2.5}$$

The normal stress jump across the interface is assumed to be balanced by a Laplace pressure term:

$$-p + Ca\,\boldsymbol{n}\cdot\boldsymbol{\tau}\cdot\boldsymbol{n} = (\nabla_s\cdot\boldsymbol{n})\sigma \quad \text{at} \quad r = H(z), \tag{2.6}$$

where $\boldsymbol{\tau}$ is the deviatoric stress. In this balance, surface viscosities have been neglected. However, their effect is discussed in the concluding section of this article.

Finally, the tangential stress balance requires that the shearing by the viscous fluid be balanced by the Marangoni stress.

$$Ca\,\boldsymbol{t}\cdot\boldsymbol{\tau}\cdot\boldsymbol{n} = -\boldsymbol{t}\cdot\nabla_s\sigma \quad \text{at} \quad r = H(z). \tag{2.7a}$$

Since the surface tension σ is a function of the surface concentration Γ, the tangential stress balance can be written:

$$Ca\,\boldsymbol{t}\cdot\boldsymbol{\tau}\cdot\boldsymbol{n} = E\,\boldsymbol{t}\cdot\nabla_s\Gamma \quad \text{at} \quad r = H(z). \tag{2.7b}$$

The elasticity number, E:

$$E = \frac{-\mathrm{d}\sigma'}{\mathrm{d}\Gamma'}\bigg|_{eq} \frac{\Gamma'_{eq}}{\sigma'_{eq}},$$

is a measure of the ratio of Marangoni stresses to interfacial tension in the system. Because of the Marangoni stress, the distribution of surfactant along the interface must be determined in order to complete the problem formulation.

2.2. *Surfactant mass transfer*

The most general mass transfer equations are stated here. They will be used below to find the relevant scalings of the dimensionless groups for the sorption-controlled limit.

At equilibrium, the distribution of surfactant between the interface and the bulk is governed by an adsorption isotherm, in which the adsorptive flux of surfactant $P(C, \Gamma)$ is balanced by the desorptive flux $Q(C, \Gamma)$:

$$P(C = 1, \Gamma = 1) = Q(C = 1, \Gamma = 1). \tag{2.8}$$

Under these conditions, the surface tension is at equilibrium. These fluxes are made dimensionless by the quantity $\Gamma'_{eq}\sigma'_{eq}/(R'\mu')$.

The concentration in the bulk liquid $C(r, z)$ is governed by a balance of convection and diffusion:

$$Pe\,\boldsymbol{u}\cdot\nabla C = \nabla^2 C, \tag{2.9a}$$

or, isolating the velocity dependence in the capillary number,

$$Ca\,\Lambda\boldsymbol{u}\cdot\nabla C = \nabla^2 C. \tag{2.9b}$$

The bulk Péclet number Pe:

$$Pe = U'R'/D',$$

gives the relative rates of convective to diffusive mass transfer in the bulk system. In this expression, D' is the bulk surfactant diffusivity. This group can be written as a product of $Ca\,\Lambda$, where Λ is:

$$\Lambda = \frac{\sigma'_{eq}R'}{D'\mu'}.$$

The bulk concentration obeys a no-flux condition at the tube wall:

$$\frac{\partial C}{\partial r} = 0 \quad \text{at} \quad r = 1; \tag{2.10}$$

and tends to a uniform value both far ahead of the bubble and in the long, cylindrical region:

$$\lim_{z\to\infty} C(r, z) = 1, \tag{2.11}$$

$$\lim_{z\to-\infty} C(r, z) = C_{film}. \tag{2.12}$$

The surface concentration is determined by the balance of surface diffusion, surface convection and the mass flux S from the fluid sublayer:

$$Ca\,\nabla_s\cdot(\Gamma\boldsymbol{u}_s) - \frac{1}{\Lambda_s}\nabla_s^2\Gamma = S \quad \text{at} \quad r = H(z), \tag{2.13}$$

where $\boldsymbol{u}_s$ is the surface velocity, defined by:

$$\boldsymbol{u}_s = (\boldsymbol{I}-\boldsymbol{nn})\cdot\boldsymbol{u}.$$

The group Λ_s is:

$$\Lambda_s = \frac{\sigma'_{eq}R'}{D'_s\mu'},$$

where D'_s is the surface diffusivity. As for the bulk phase, Λ_s can be related to a surface Péclet number. The flux S is determined by two processes that occur in series: diffusion of surfactant to the sublayer, followed by adsorption onto the interface:

$$S = -\frac{1}{\lambda\Lambda}\boldsymbol{n}\cdot\nabla C \quad \text{at} \quad r = H(z), \tag{2.14a}$$

and

$$S = P(C,\Gamma)-Q(C,\Gamma) \quad \text{at} \quad r = H(z). \tag{2.14b}$$

where the dimensionless adsorption depth λ:

$$\lambda = \frac{\Gamma'_{eq}}{C'_{eq}R'},$$

is a measure of the distance beneath the interface that is depleted by surfactant adsorption. As this depth approaches zero (for example, when the bulk concentration of surfactant is high) S becomes decoupled from the bulk diffusive flux.

At equilibrium, S is zero, the bulk concentration is uniform, and the rates of adsorption and desorption balance as required by the adsorption isotherm (2.8). Expanding S in a Taylor series about the equilibrium state and retaining first-order terms, the balance becomes:

$$S = -\frac{1}{\lambda\Lambda}\boldsymbol{n}\cdot\nabla C = K_c(C-1)+K_\Gamma(\Gamma-1) \quad \text{at} \quad r = H(z), \tag{2.14c}$$

where K_c is the bulk adsorption number:

$$K_c = \frac{C_{eq}}{\Gamma_{eq}}\frac{\left.\frac{\partial P'}{\partial C'}\right|_{eq}-\left.\frac{\partial Q'}{\partial C'}\right|_{eq}}{\sigma'_{eq}/R'\mu'},$$

a measure of the dependence of the net sorptive flux on bulk concentration gradients. Similarly, K_Γ, the surface adsorption number:

$$K_\Gamma = \frac{\left.\frac{\partial P'}{\partial \Gamma'}\right|_{eq}-\left.\frac{\partial Q'}{\partial \Gamma'}\right|_{eq}}{\sigma'_{eq}/R'\mu'},$$

is a measure of the dependence of the net sorptive flux on surface concentration gradients. The groups K_c and K_Γ are a measure of the characteristic rate of adsorptive–desorptive exchange. For example, the ratio of K_Γ/Ca is the ratio of characteristic sorptive flux caused by a surface concentration gradient to the surface convective flux in the system. These groups are not independent, but are implicitly related by the adsorption isotherm (2.8).

Finally, in the thin film region of the bubble, the surface concentration must tend to some uniform value in equilibrium with the bulk concentration there:

$$\lim_{z\to-\infty} \Gamma(z) = \Gamma_{film}. \tag{2.15}$$

These are the complete governing equations.

2.3. *Dimensionless groups in related studies*

The scales used in this article were chosen so that velocity is isolated in Ca, with the remaining dimensionless groups containing only parameters that characterize the physical chemistry and geometry of the system.

Some of the dimensionless groups differ from those adopted in the study of Ratulowski & Chang. Throughout their analysis, the clean interface value for the surface tension is used instead of the equilibrium value. Furthermore, they chose to scale bulk concentration with C'_∞, a characteristic bulk concentration, and surface concentration with $R'C'_\infty$. Because of this choice of scalings, their adsorption depth λ is implicitly unity.

The elasticity number based on clean surface values appears in the Ratulowski & Chang (1990) analysis as a Marangoni number. We prefer to call this group the elasticity number, reserving the term Marangoni number for its more traditional definition as the ratio of E/Ca, which is a measure of Marangoni to viscous stresses in the system.

Finally, in their study, the adsorption isotherm (2.8) is linearized in the limit of small adsorption. This expression is used to define the Stanton number, St, as a measure of sorption kinetic barriers. In terms of quantities defined in our study, the Stanton number is:

$$St = \frac{\left(\dfrac{\partial P'}{\partial \Gamma'} - \dfrac{\partial Q'}{\partial \Gamma'}\right)\Big|_{\Gamma'=0}}{U'/R'},$$

which is a measure of the rate of surfactant adsorption relative to surface convection for small departures from a clean interface state. The product $StCa$ is an adsorption number for small departures from clean interface conditions, analogous to the bulk or surface adsorption numbers defined above.

3. Determination of the magnitude of the dimensionless parameters

Both bulk surfactant mass transfer and surface diffusion are assumed to be negligible in this analysis, an assumption that is valid only for certain ranges of the mass transfer and interface related dimensionless groups.

This study emphasizes the role of adsorptive–desorptive mass transfer in the case where the mass transfer and flow field are strongly coupled. Therefore, the elasticity number E and the sorption kinetic parameters K_C and K_Γ are leading order, i.e.

$$E = O(1),$$
$$K_C = O(1),$$
$$K_\Gamma = O(1).$$

For the situation where the bulk concentration is uniform, only E and K_Γ play a role in determining the behaviour of the system. Since experimental evidence indicates that

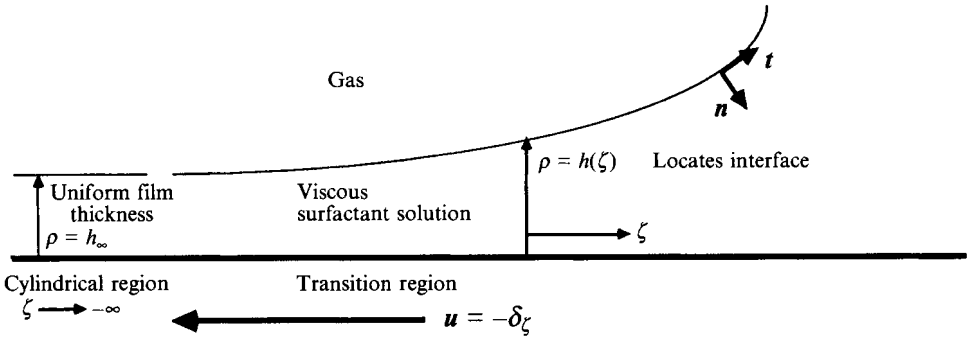

FIGURE 3. The rescaled coordinates for the transition region include ρ, which measures the distance from the tube wall toward the tube centre, ζ, which measures the axial location in the transition region. The origin of the axial coordinate is shifted a distance $-l$ from the origin of the hemispherical cap. The position of the interface is given by $\rho = h(\zeta)$.

D' and D'_s are of the same order of magnitude (see, for example, the review by Agrawal & Neuman 1988) A and A_s are assumed to have the same order in this analysis. Their magnitude, and those of the remaining dimensionless groups can be identified by considering the mass transfer equations for each region of the flow field. This requires that the scalings of the equations in each of the regions be understood.

3.1. *Scalings and regions*

Equations (2.1)–(2.7) accurately describe the behaviour of the hemispherical cap region. In the transition region, however, the interface must bend from a nearly cylindrical geometry to a nearly spherical shape. This requires that viscous tractions must be retained in the equations of motion, and that the governing equations be rescaled.

The proper transition region scalings have been derived in detail by Bretherton and by Park & Homsy and are used here without proof. The rescaled coordinates, shown in figure 3, include ρ, a stretched distance from the tube wall, and ζ, a stretched axial coordinate, which measures the distance from the origin of the transition region. This origin is shifted a distance l from the leading pole of the bubble, which is determined as part of the solution. In this coordinate system, the thickness of the liquid film is denoted by $h(\zeta)$. The transverse velocity v_ρ must also be stretched in order that the equation of continuity be satisfied. The rescaled variables are:

$$\rho = \frac{(1-r)}{Ca^{2/3}}, \tag{3.1}$$

$$\zeta = \frac{(z+1)}{Ca^{1/3}}, \tag{3.2}$$

$$h(\zeta) = \frac{(1-H(z))}{Ca^{2/3}}, \tag{3.3}$$

$$v_\rho = \frac{-v_r}{Ca^{1/3}}. \tag{3.4}$$

Neither the axial velocity v_ζ nor the pressure need be rescaled. In terms of these variables, the equations of motion reduce to the lubrication equations to leading order.

These scales require that the perturbation expansion of any unknown X, must occur in powers of $Ca^{1/3}$:

$$X = \sum Ca^{n/3} X_{(n)}. \tag{3.5}$$

3.2. *Hemispherical cap region*

The unknowns in (2.1)–(2.7) are expanded according to (3.5). It follows from (2.1) that the pressure and velocity are then decoupled up to $O(Ca)$. The tangential stress balance (2.7*b*) requires that the lowest-order perturbation in the surface concentration must be $O(Ca)$ in order that the tangential stresses remain bounded. Because the elasticity number E is $O(1)$, the surface tension also departs from its equilibrium at $O(Ca)$. Therefore, as in the Bretherton study, the normal stress balance (2.6) reduces to the Laplace–Young equation:

$$-p = (\nabla_s \cdot \boldsymbol{n}) + O(Ca) \quad \text{at} \quad r = H(z). \tag{3.6}$$

The integration of (3.6) shows the interface location in this region to be a hemispherical cap of radius $\frac{1}{2}p$:

$$H(z) = \frac{2}{p}(1 - [\tfrac{1}{2}pz + 1]^2)^{\frac{1}{2}} + O(Ca). \tag{3.7}$$

Together (3.7) and (2.1) require that any changes in pressure from the static pressure before order $O(Ca)$ must be caused by effects of the flow field on the curvature of the interface.

The tangential stress balance (2.7) does not simplify to the Bretherton clean interface balance. Rather, the Marangoni stress term balances the viscous shearing to leading order. This does not complicate the analysis since, according to (3.7) the flow field does not influence the leading-order pressure and interfacial shape.

3.3. *Mass transfer in the hemispherical cap region*

The mass transfer equations for this region (2.8)–(2.15) reduce to the sorption controlled limit only when the dimensionless groups obey certain upper bounds. The bulk mass balance (2.9*b*) requires that Λ (and therefore Λ_s) be $O(Ca^{-2/3})$ in order that bulk convective flux be neglected. The normal diffusive flux to the interface is zero to leading order if the product $\lambda\Lambda$ is $O(Ca^{1/3})$ according to (2.14*a*). Finally, since the surface Laplacian of the surface concentration is $O(Ca)$, and Λ_s is $O(Ca^{-2/3})$, the surface diffusivity term in (2.13) is negligible. Adopting these scales, the leading-order bulk concentration in the hemispherical cap is uniform and the mass transfer in this region is adsorption–desorption controlled.

3.4. *Transition region equations*

Adopting the rescaled variables given in (3.1)–(3.4), the equations of motion for the transition region reduce to the lubrication equations, and the tangential stress balance is:

$$Ca^{2/3}\frac{\partial v_\zeta}{\partial \rho} = E\frac{\partial \Gamma}{\partial \zeta} + O(Ca) \quad \text{at} \quad \rho = h(\zeta). \tag{3.8}$$

In order that the viscous shearing on the interface remain bounded, (3.8) requires that the surface concentration in the transition region depart from its equilibrium value at $O(Ca^{2/3})$. The surface tension also departs from equilibrium at this order, and the normal stress balance becomes:

$$-p = \left(1 + \frac{\mathrm{d}^2 h}{\mathrm{d}\zeta^2}\right)\{1 + O(Ca^{2/3})\} \quad \text{at} \quad \rho = h(\zeta). \tag{3.9}$$

3.5. *Mass transfer in the transition region*

As in §3.3 the mass transfer equations are used to specify the upper bounds on the dimensionless groups. In terms of the rescaled variables, the bulk mass balance (2.9*b*) becomes:

$$Ca^2\Lambda\left[v_\rho\frac{\partial C}{\partial\rho}+v_\zeta\frac{\partial C}{\partial\zeta}\right]=\frac{\partial^2 C}{\partial\rho^2}+Ca^{2/3}\frac{\partial^2 C}{\partial\zeta^2}. \tag{3.10}$$

The flux condition at the interface (2.14*c*) becomes:

$$\frac{\partial C}{\partial\rho}+Ca^{2/3}\frac{\partial h}{\partial\zeta}\frac{\partial C}{\partial\zeta}=Ca^{2/3}\lambda\Lambda[K_C(1-C)+K_\Gamma(1-\Gamma)] \quad \text{at} \quad \rho=h(\zeta). \tag{3.11}$$

Similarly, equating (2.13) and the diffusive flux (2.14*a*), the interfacial mass flux can be written:

$$\frac{\partial C}{\partial\rho}+Ca^{2/3}\frac{\partial h}{\partial\zeta}\frac{\partial C}{\partial\zeta}=\lambda\Lambda\,Ca^{2/3}\left[Ca^{2/3}\frac{\partial(\Gamma u_s)}{\partial\zeta}-\frac{1}{\Lambda_s}\frac{\partial^2\Gamma}{\partial\zeta^2}\right] \quad \text{at} \quad \rho=h(\zeta). \tag{3.12}$$

According to (3.10) the bulk convective flux can be neglected for Λ of $O(Ca^{-1})$ (thereby also specifying Λ_s). The diffusive flux (3.11) to the interface is negligible if the group $\lambda\Lambda$ is of $O(Ca^{1/3})$. For these scales, the surface diffusive flux in (3.12) is negligible and the bulk concentration remains uniform throughout both the transition and cylindrical film regions. The mass transfer is therefore sorption controlled, and is governed by the simplified mass balance:

$$K_\Gamma(1-\Gamma)=Ca^{2/3}\frac{\mathrm{d}(\Gamma u_s)}{\mathrm{d}\zeta} \quad \text{at} \quad \rho=h(\zeta). \tag{3.13}$$

3.6. *Cylindrical region*

In the cylindrical region the film thickness, velocity and concentration fields have uniform values. When bulk diffusion is negligible, the concentration remains uniform in all three regions, and the limiting values for the transition region variables are simply:

$$\lim_{\zeta\to-\infty}\Gamma=1, \tag{3.14}$$

$$\lim_{\zeta\to-\infty}u_s=-1, \tag{3.15}$$

$$\lim_{\zeta\to-\infty}h=h_\infty. \tag{3.16}$$

3.7. *Ordering of the diffusion-related dimensionless groups*

In order to neglect bulk phase mass transfer for the entire system, the stronger restrictions on the bulk diffusive flux flow must be adopted. For Λ and Λ_s, these are the restrictions imposed by the hemispherical region;

$$\Lambda=\Lambda_s=O(Ca^{-2/3}).$$

For the adsorption depth λ, these scales, combined with the transition region restriction on the product $\lambda\Lambda$ require that:

$$\lambda=O(Ca).$$

Adopting these scalings, the flux of surfactant in the system is sorption controlled and the bulk concentration is unity everywhere.

Expanding each of the unknowns according to (3.5), the asymptotic equations that govern each region are developed and discussed in the next section.

4. Asymptotic expansions

4.1. *Hemispherical cap region*

As discussed in §3.2, the concentration, surface tension and pressure fields are determined up to $O(Ca)$ in this region. According to (3.7) the pressure to $O(Ca^{2/3})$ is determined by the interfacial shape, which is found by matching the hemispherical cap to the transition region. The matching between the two regions is described in §4.4.

4.2. *Transition region*

To leading order the transition region is governed by the lubrication equations:

$$\frac{\mathrm{d}p_{(0)}}{\mathrm{d}\zeta} = \frac{\partial^2 v_{\zeta(0)}}{\partial \rho^2}, \tag{4.1}$$

subject to the integral mass balance:

$$\int_0^{h_{(0)}(\zeta)} v_{\zeta(0)}\,\mathrm{d}\rho = -h_\infty. \tag{4.2}$$

The three boundary conditions at the interface $\rho = h_{(0)}(\zeta)$ are:

the tangential stress balance:

$$\frac{\partial v_{\zeta(0)}}{\partial \rho} = E\frac{\mathrm{d}\Gamma_{(2)}}{\mathrm{d}\zeta} \quad \text{at} \quad \rho = h_{(0)}; \tag{4.3}$$

the normal stress balance:

$$-p_{(0)} = 1 + \frac{\mathrm{d}^2 h_{(0)}}{\mathrm{d}\zeta^2} \quad \text{at} \quad \rho = h_{(0)}; \tag{4.4}$$

and the kinematic condition at the interface:

$$v_{\rho(0)} = \frac{\mathrm{d}h_{(0)}}{\mathrm{d}\zeta} u_{s(0)} \quad \text{at} \quad \rho = h_{(0)}. \tag{4.5}$$

The surface velocity $u_{s(0)}$ in the transition region is defined by:

$$u_{s(0)} = v_{\zeta(0)} \quad \text{at} \quad \rho = h_{(0)}. \tag{4.6}$$

Along the wall, the no-slip condition requires:

$$v_\zeta = -\delta_\zeta \quad \text{at} \quad \rho = 0. \tag{4.7}$$

Finally, the surface mass balance completes the problem formulation in this region:

$$\Gamma_{(2)} = -\frac{1}{K_\Gamma}\frac{\mathrm{d}u_{s(0)}}{\mathrm{d}\zeta} \quad \text{at} \quad \rho = h_{(0)}. \tag{4.8}$$

Integrating (4.1) subject to (4.2), (4.4) and (4.7), the equation governing the local film thickness $h_{(0)}(\zeta)$ can be determined:

$$\frac{\mathrm{d}^3 h_{(0)}}{\mathrm{d}\zeta^3} = \frac{6(1-u_{s(0)})h_{(0)} - 12h_\infty}{h_{(0)}^3}. \tag{4.9}$$

The equation governing $u_{s(0)}$ is found from equations (4.1)–(4.4) and (4.7) and (4.8) to be:

$$u_{s(0)} = \frac{1}{2} - \frac{3h_\infty}{2h_{(0)}} - \frac{E}{4K_\Gamma}\frac{\mathrm{d}^2 u_{s(0)}}{\mathrm{d}\xi^2} h_{(0)}. \tag{4.10}$$

The film equation (4.9) is identical to that obtained by Ratulowski & Chang. However, these authors find a surface velocity different from (4.10) in their bulk equilibrium model. Since the mass transfer regimes for the two studies differ, so do the tangential stress conditions that are used to derive the surface velocity equation. However, (4.9) and (4.10) are essentially the same as those originally derived by Hirasaki & Lawson.

Marangoni stresses alter the flow field through the term containing the group E/K_Γ. Furthermore (4.9) and (4.10) tend to the appropriate limits as the magnitude of E/K_Γ is varied. When E/K_Γ is $O(Ca^{1/3})$, the mass transfer and tangential stresses are decoupled to leading order. This can be caused by either of two mechanisms: either the interface is insensitive to surfactant adsorption (E of $O(Ca^{1/3})$, K_Γ of $O(1)$), or the rate of surfactant adsorptive–desorptive exchange is infinitely fast (E of $O(1)$, K_Γ of $O(Ca^{-1/3})$) so that the surface remains unperturbed from its equilibrium. For either of these cases, the interface behaves to leading order as it would in the absence of surfactant, and the clean interface equations of Bretherton are recovered where the surface tension is replaced by its equilibrium value σ'_{eq}.

The opposite extreme, E/K_Γ of $O(Ca^{-1/3})$ can be approached either because of a strong dependence of surface tension on surfactant adsorption (E of $O(Ca^{-1/3})$, K_Γ of $O(1)$), or because the adsorbed surfactant behaves like an insoluble monolayer, with the rate of adsorptive–desorptive exchange tending to zero (E of $O(1)$, K_Γ of $O(Ca^{1/3})$). In order that the surface velocity (4.10) remain bounded in this limit, the second derivative of $u_{s(0)}$ must go to zero. This condition, along with (3.15) which dictates that the surface velocity in the cylindrical region be uniform, requires that $u_{s(0)}$ remain constant and equal to the wall velocity value throughout the transition region. In this limit, the film thickness equation becomes:

$$\frac{\mathrm{d}^3 h_{(0)}}{\mathrm{d}\xi^3} = 12\frac{(h_{(0)} - h_\infty)}{h_{(0)}^3}. \tag{4.11}$$

which is simply the maximum surfactant effect model (cf. Herbolzheimer 1987; Chang & Ratulowski 1987) for this flow field.

The coupled differential equations (4.9) and (4.10) with unknowns $h_{(0)}$, h_∞, and $u_{s(0)}$ describe the dynamics of the transition region. Their solution requires proper matching conditions with the uniform film and hemispherical cap regions.

To facilitate their integration, these equations are recast in canonical forms in terms of $j(\xi)$, where j and ξ are:

$$j(\xi) = \frac{h_{(0)}}{h_\infty}, \quad \xi = \frac{(\xi - s)}{h_\infty}, \tag{4.12}$$

and s is an arbitrary shift of origin. In terms of these variables, (4.9) and (4.10) become:

$$\frac{\mathrm{d}^3 j}{\mathrm{d}\xi^3} = \frac{6[(1-u_{s(0)})j - 2]}{j^3}, \tag{4.13}$$

and

$$u_{s(0)} = \frac{1}{2} - \frac{3}{2j} + \frac{M}{4}\frac{\mathrm{d}^2 u_{s(0)}}{\mathrm{d}\xi^2} j, \tag{4.14}$$

where M is defined by:

$$M = \frac{E}{K_\Gamma h_\infty}. \tag{4.15}$$

This group contains the film thickness in the cylindrical region, h_∞. While h_∞ is unknown *a priori*, it is bounded below by the Bretherton wetting-layer thickness and above by the maximum surfactant effect film thickness:

$$1.34 \leqslant h_\infty \leqslant 4^{2/3}\,1.34.$$

in terms of transition region scales. Since h_∞ is always an $O(1)$ quantity, the magnitude of M indicates the magnitude of the Marangoni effects in the flow field.

4.3. *Matching with the cylindrical region*

Equations (3.14)–(3.16) require that the transition region velocity, concentration and film thickness at large, negative ξ must tend to their cylindrical region values. Therefore, in this limit, j and $u_{s(0)}$ must tend to the limits:

$$\lim_{\xi \to -\infty} j = 1, \tag{4.16}$$

$$\lim_{\xi \to -\infty} u_{s(0)} = -1. \tag{4.17}$$

According to the surface mass balance (4.8), deviations in the surface concentration from its equilibrium are proportional to the derivative of the surface velocity. Therefore (4.17) implicitly forces the surface concentration to approach its equilibrium value in this limit.

Conditions for the departure of the transition region equations from their thin film values are found by expanding (4.13) and (4.14) about the limiting values of (4.16) and (4.17) and retaining only first-order terms. The linearized equations are:

$$\tfrac{1}{4}M\left[\frac{\mathrm{d}^5(j-1)}{\mathrm{d}\xi^5} - \frac{12\mathrm{d}^2(j-1)}{\mathrm{d}\xi^2}\right] - \left[\frac{\mathrm{d}^3(j-1)}{\mathrm{d}\xi^3} - 3(j-1)\right] = 0, \tag{4.18}$$

$$\tfrac{1}{4}M\frac{\mathrm{d}^2(u_{s(0)}+1)}{\mathrm{d}\xi^2} - (u_{s(0)}+1) = -\tfrac{3}{2}(j-1). \tag{4.19}$$

Substituting

$$j = 1 + \exp(m_i \xi)$$

into (4.18) results in a fifth-order algebraic equation for the eigenvalues m_i. These eigenvalues, which are functions of M, have been determined numerically for the range of M from 10^{-2} to 10^6. For each value of M there are two positive real eigenvalues. The remaining three eigenvalues consist of one that is real and negative and a complex conjugate pair with negative real parts. Since both j and $u_{s(0)}$ must remain bounded as ξ becomes large and negative, only the two eigenvalues with positive real parts, m_1 and m_2, can contribute to the initial departure of j and $u_{s(0)}$ from the uniform film region. The solutions for j and $u_{s(0)}$ at large negative ξ are therefore:

$$j(\xi) = 1 + c_0 \exp(m_1 \xi) + c_1 \exp(m_2 \xi), \tag{4.20}$$

$$u_{s(0)} = -1 - \frac{6}{M}\left[\frac{c_0 \exp(m_1 \xi)}{m_1^2 - \dfrac{4}{M}} + \frac{c_1 \exp(m_2 \xi)}{m_2^2 - \dfrac{4}{M}}\right] + c_2 \exp\left(\left(\frac{4}{m}\right)^{1/2} \xi\right). \tag{4.21}$$

These equations are used to initiate the integration of (4.13) and (4.14) at some negative value of ξ. Because of the arbitrary shift of origin s, one of the constants, say c_0, can arbitrarily be set equal to 1.

4.4. *Matching with the capillary statics region*

The remaining unknowns, c_1, c_2, l, h_∞ and p are determined by matching the profiles for h and Γ_{TR} at the outer edge of the transition region to the cap region profiles H and Γ_{HC} at the inner limit of the cap region. The matching conditions are:

$$\lim_{\zeta\to\infty}(1-Ca^{2/3}h_{(0)}(\zeta)) = \lim_{z\to-1} H(z), \tag{4.22}$$

$$\lim_{\zeta\to\infty}\Gamma_{TR} = \lim_{z\to-1}\Gamma_{HC}, \tag{4.23}$$

where the subscripts TR and HC denote transition region and hemispherical cap variable, respectively. The matching of the film profiles (4.22) is that used by Bretherton and formalized by Park & Homsy. Their results for this condition are recapitulated briefly below.

At large ξ, the film thickness becomes large, and (4.13) yields a quadratic expression for j:

$$j = \tfrac{1}{2}B_0\xi^2 + B_1\xi + B_2, \tag{4.24}$$

or, in terms of $h_{(0)}(\zeta)$:

$$h_{(0)}(\zeta) = \frac{B_0}{2h_\infty}(\zeta+s)^2 + B_1(\zeta+s) + B_2 h_\infty. \tag{4.25}$$

For the profiles in the outer region, (3.7) is expanded in a Taylor series about $z=-l$ and expressed in inner variables. Term by term matching at $O(1)$ and $O(Ca^{1/3})$ gives:

$$\tfrac{1}{2}p_{(0)} = -1, \tag{4.26}$$

$$l = 1, \tag{4.27}$$

$$p_{(1)} = 0. \tag{4.28}$$

Equation (4.26) states that the leading-order pressure in the hemispherical cap region is determined by the equilibrium surface tension. Consequently, the radius of the hemispherical cap is equal to the tube radius to leading order. Equation (4.27) fixes the origin of the transition region one radial distance away from the tip of the hemisphere. Finally, the $Ca^{1/3}$ contribution to the pressure is zero. Matching $O(Ca^{2/3})$ terms, the leading-order correction to the pressure along with the thickness of the wetting layer in the thin film region h_∞ can be resolved:

$$p_{(2)} = -B_2B_0 + \tfrac{1}{2}B_1^2, \tag{4.29}$$

$$h_\infty = B_0. \tag{4.30}$$

Finally, matching transition region and hemispherical cap region surface concentration profiles at each order of $Ca^{1/3}$, equation (4.23), together with the surface mass balance, equation (4.8) requires that:

$$\lim_{\zeta\to\infty}\Gamma_{(2)_{TR}} = \lim_{\zeta\to\infty}\frac{\mathrm{d}u_{s(0)}}{\mathrm{d}\zeta} = 0. \tag{4.31}$$

4.5. *Integration*

The integration of (4.13) and (4.14) is initialized at some finite, negative value of ξ, ξ_0, using (4.20) and (4.21). These initial conditions are functions of the unknowns constants c_1 and c_2. Values of c_1 and c_2 must be chosen so that the initial deviation of

both $u_{s(0)}$ and j from their cylindrical region values is small. In addition, the constants must allow the integration of (4.13) and (4.14) to large ξ at which j behaves like a quadratic, and matching condition (4.31) is obeyed. These boundary conditions allow the determination of c_1 and c_2, and thus a unique solution for j and $u_{s(0)}$ at each value of M.

Since the boundary conditions occur at either end of the integration path, shooting methods are required. Appropriate guesses for the unknown constants are made at the beginning of the integration. Both ξ_0 and c_1 are chosen so that

$$(j(\xi_0)-1) < 0.01. \tag{4.32}$$

The equations are integrated using a Bashforth–Adams routine to some final value ξ_f of ξ, chosen so that

$$j > 900 \tag{4.33}$$

at the end of the path. Values of c_1 and c_2 are considered satisfactory if

$$\frac{\mathrm{d}u_{s(0)}}{\mathrm{d}\xi}(\xi_f) < 10^{-5}. \tag{4.34}$$

For all of the converged values presented in this paper, the final value for j was sufficiently large that

$$\frac{\mathrm{d}^3 j}{\mathrm{d}\xi^3} = O(10^{-9}). \tag{4.35}$$

An iterative procedure is needed in order to find satisfactory values for c_1 and c_2. Before an initial integration can be performed, it is necessary to find a value for c_2 that, given c_1, allows the equations to be integrated. This requires some *a priori* knowledge of the behaviour of the system for unacceptable values of c_2. Values of c_2 that are too small (large) cause u_{s0} to become large and negative (positive). The system of equations is too sensitive to c_2 for straightforward predictor–corrector methods to be effective. Therefore, an interval halving scheme was used to find appropriate values of c_2.

The search routine involves finding c_2 for a fixed value of c_1. A value for c_1 is considered acceptable if, by choosing a smaller deviation from the thin film (i.e. a smaller guess for c_1), the values for h_∞ and p_2, found from a converged solution, change by less than 1%. If this is not the case, a new value for c_1 is adopted, and the convergence procedure is begun again. For all of the converged values presented in this paper, initial departure of j from its cylindrical region value obey (4.32) and initial departures of u_{s0} obey:

$$(u_{s(0)}(\xi_0)+1) < 0.075. \tag{4.36}$$

Once acceptable values for c_1 and c_2 are found, the profile for the film thickness should obey (4.24) at large values of j. For $j > 400$, the converged film thickness profile is fit to a quadratic allowing values for the wetting-layer thickness and leading-order pressure corrections to be evaluated. The results of the integration and matching procedures are discussed below.

5. Results and discussion

5.1. *Results*

As discussed in §1 and sketched in figure 2, a depletion of surfactant is anticipated in the region of the stagnation ring. This depletion is shown in figure 4, where the leading-order deviation in the surface concentration from its equilibrium for M equal to 0.5

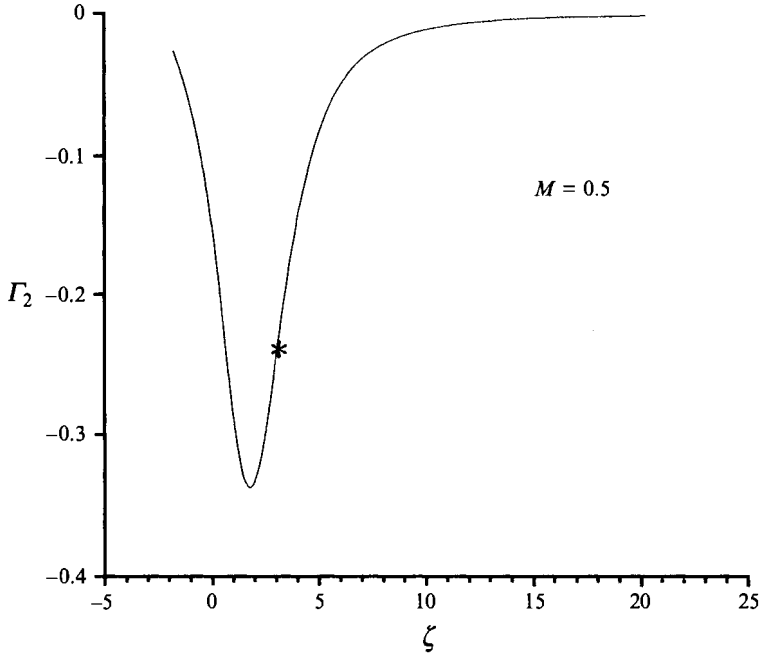

FIGURE 4. The transition region surface concentration deviation Γ_2 *vs.* ζ is shown for $M = 0.5$ and $K_\Gamma = 1.0$. The symbol * marks the location of the stagnation ring in this figure.

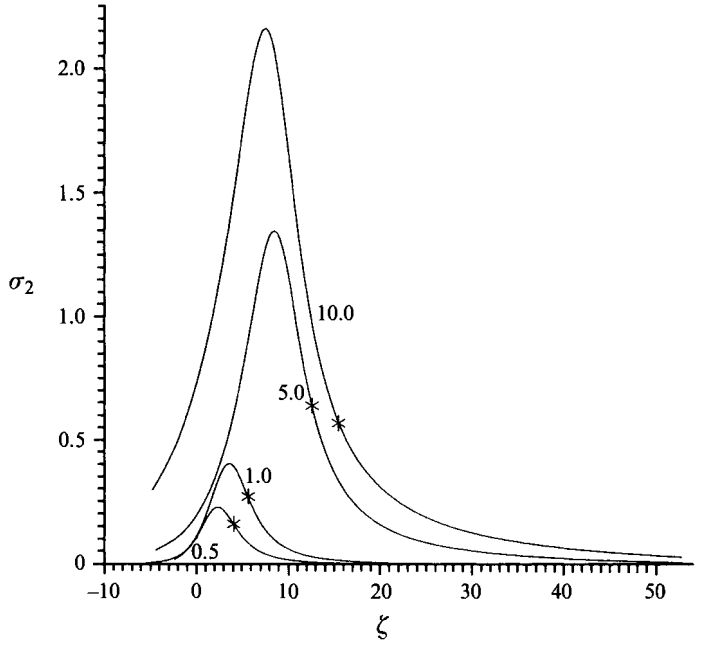

FIGURE 5. The transition region surface tension deviation σ_2 *vs.* ζ for various M values. The symbol * marks the location of the stagnation ring in this figure.

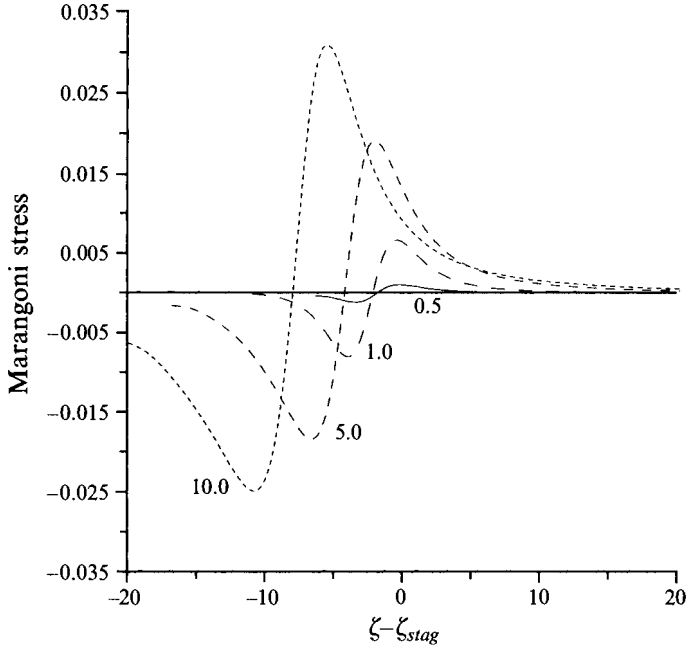

FIGURE 6. The Marangoni stress is shown *vs.* ζ for various M values. The symbol * marks the location of the stagnation ring in this figure.

and K_Γ equal to 1.0 is shown as a function of the transition region axial coordinate, ζ. The asterisk indicates the location of the stagnation ring. The corresponding surface tension deviation for the same M value is simply:

$$\sigma_2 = -E\Gamma_2.$$

Surface tension deviations as a function of the axial coordinate are shown in figure 5 for different M values. The minimum in the surface concentration, and therefore the maximum in the surface tension precedes the location of the stagnation ring. The corresponding Marangoni stress exerted by the interface on the fluid is shown in figure 6. The Marangoni stress pulls toward the point of maximum surfactant depletion. As M increases, rather than simply slowing the surface velocity, the flow field reacts to the increased drag by displacing the site of maximum surfactant depletion to regions of larger film thickness. Negative surface concentration gradients are therefore favoured at larger values of ζ. Together, (4.8) and (4.10) show that this favours the displacement of the stagnation ring toward the cap region and out of the transition region. Surface velocity profiles are shown in figure 7 as a function of film thickness $h_{(0)}$ in the transition region. For $M < 1$, the surface velocity departs only slightly from the clean interface profile, for which the stagnation ring occurs for $h_{(0)}$ equal to $3h_{\infty Br}$. As M increases between 1 and 10, the stagnation ring migrates out to larger film thicknesses. For $M > 10$, there is no longer a stagnation ring in the transition region. Rather, the surface velocity remains negative throughout the region, departing progressively less from -1.0 as M is increased over several orders of magnitude, thus approaching the maximum surfactant effect limit.

The film thickness profiles in the transition region are shown as a function of ζ in figure 8. The film profiles have been shifted axially so that their shapes can be clearly seen. The asymptote of the film profiles at negative ζ, i.e. the wetting-layer thickness in the uniform film region, increases with M. In addition, as expected, each profile

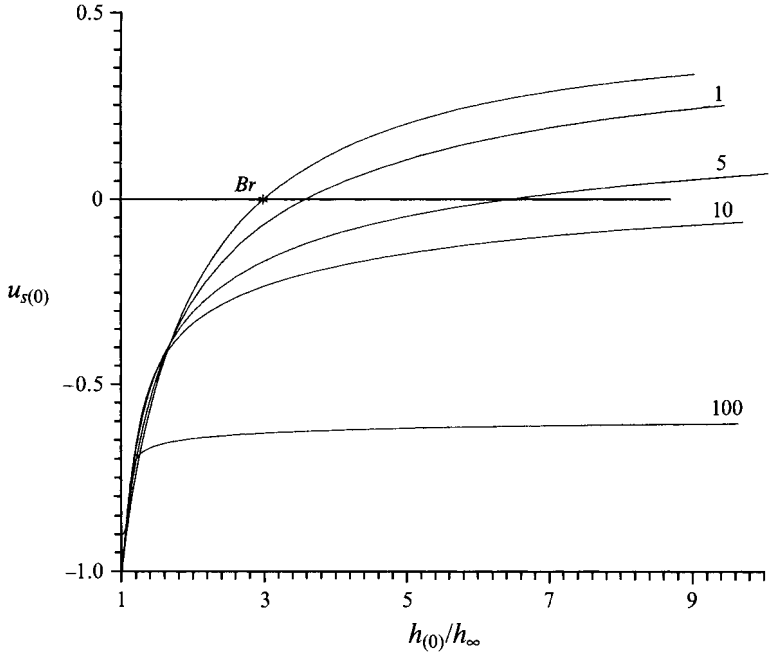

FIGURE 7. The surface velocity $u_{s(0)}$ *vs.* film thickness $h_{(0)}(\zeta)$ for various M values is shown. As M increases from zero, the stagnation ring is displaced toward the hemispherical cap region. This migration of the stagnation ring continues until, for $M > 10$, the surface velocity remains negative throughout the transition region.

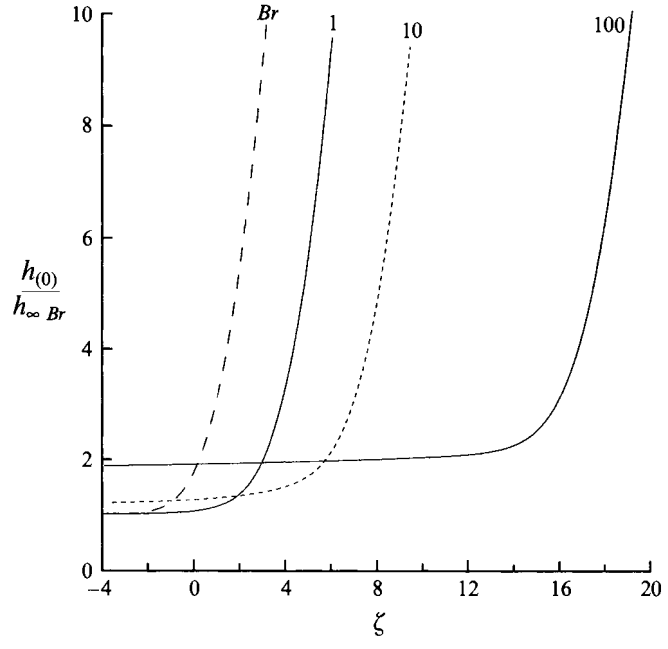

FIGURE 8. The transition region interfacial profile scaled by the Bretherton uniform film thickness, $h_{(0)}(\zeta)/h_{\infty Br}$ is shown for different values of the Marangoni stress parameter M. The curves have been displaced axially so that their shapes can be clearly seen.

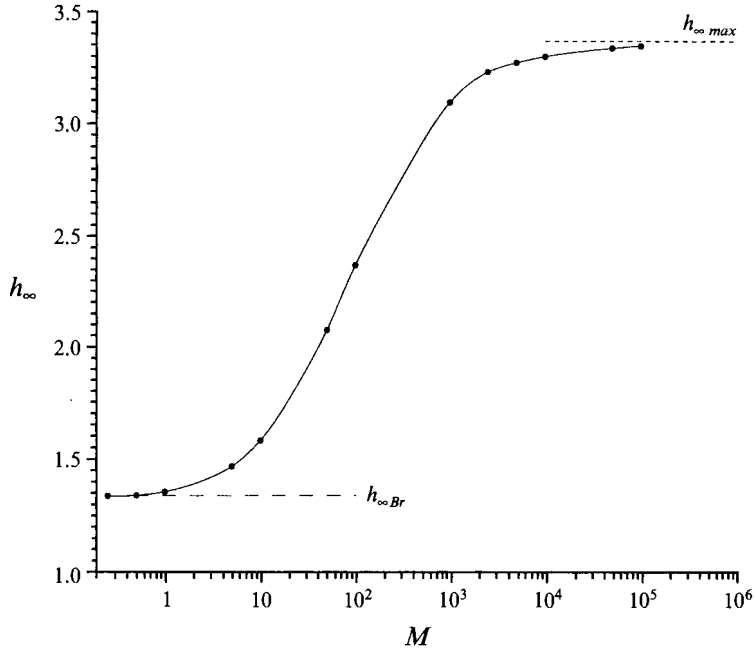

FIGURE 9. The uniform film thickness in the cylindrical region h_∞ is shown as a function of M. The film thickness is bounded below by the Bretherton value and above by the maximum surfactant effect value.

grows quadratically at large ζ. It is the shape of these parabolic regions that determines both the leading-order correction to the pressure p_2, and the uniform wetting layer thickness h_∞.

Figure 9 shows the dependence of the uniform film thickness h_∞, on the parameter M. For small M, h_∞ asymptotes to the Bretherton value from above (i.e. the uniform wetting layer is always thicker than the clean interface value). As M increases, h_∞ increases monotonically, approaching its upper bound, the 'maximum surfactant effect'.

The total pressure drop between the uniform film and hemispherical cap region is:

$$\Delta p = 1 + Ca^{2/3} p_2.$$

The first term in this expression is due to the change in curvature between the two regions, while the second is linked with viscous and Marangoni effects. The behaviour of p_2 is shown in figure 10, also as a function of increasing M. For weak Marangoni effects (small M), p_2 is only slightly in excess of the Bretherton value, which is the additional pressure drop required to overcome viscous shearing in the transition region. As M increases, the value of p_2 also increases monotonically, so that the combination of viscous and Marangoni effects requires higher pressures to aspirate the bubble. At large M, p_2 also approaches an upper bound, the 'maximum surfactant effect'.

5.2. *Discussion*

5.2.1. *Uniform wetting layer thickness*

In their study of the effects of surfactant adsorption on this flow geometry Ratulowski & Chang showed that higher pressure drops and thicker films result from hindered bulk mass transfer. The present study establishes that Marangoni stresses that

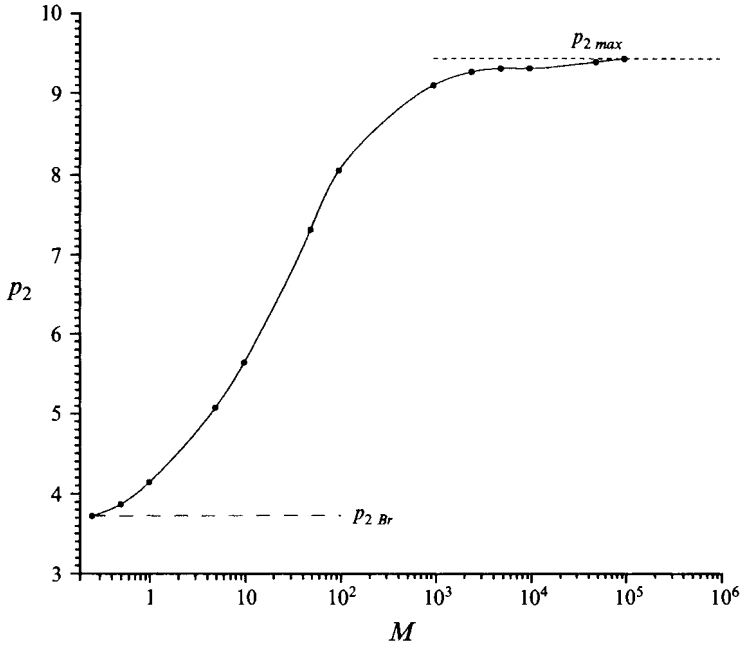

FIGURE 10. The leading-order correction to the pressure p_2 is shown as a function of the Marangoni stress parameter M. The lower bound is the Bretherton value; the upper bound is the maximum surfactant effect value.

result from hindered sorptive exchange also cause thicker wetting layers and elevated pressure drops. Furthermore, for both cases the wetting layer thicknesses and leading-order correction to the pressure are bounded below by the clean interface behaviour, and above by the 'maximum surfactant effect'.

These trends can be anticipated by examining the tangential stress balance. The tangential stress balance in the transition region can be written:

$$-\frac{(u_{s(0)}+1)}{h_{(0)}}+\frac{\mathrm{d}^3 h_{(0)}}{\mathrm{d}\zeta^3}\frac{h_{(0)}}{2}=\frac{1}{Ca^{2/3}}\frac{\mathrm{d}\sigma}{\mathrm{d}\zeta}, \tag{5.1}$$

where the right-hand side of this expression is the Marangoni stress. Moving along the bubble from the thin film into the transition region, the surface tension gradient is positive. Consequently, the left-hand side of this expression must be larger than it would be in the case where the interface is stress-free. There are three trends that favour an increase in the left-hand side of (5.1): smaller deviations in the surface velocity $u_{s(0)}$ from its uniform film value, thicker local films and larger rates of change of the curvature. This balance indicates that surfactant effects always result in thicker films and higher pressures for this flow field, independent of the mass transfer mechanism.

5.2.2. *Effects of surface viscosities*

Interfaces have been postulated to resist shear and dilatation, both through the Marangoni stress discussed above and through surface viscosities that resist dilatation and shear. The equations describing the dynamics of an interface with Newtonian intrinsic stress behaviour were derived by Scriven (1960). Values for the coefficients of surface dilatational viscosity, κ', and surface shear viscosity, ϵ', have been measured with a variety of interfacial viscometers which subject the interface to pure shear or to both shear and dilatation (see e.g. Jiang, Chen & Slattery 1983; Djabbarah & Wasan

1982; Wei & Slattery 1976). These parameters depend upon the local concentration and structure of adsorbed surfactant in a manner that is not yet well understood. However, their dependence on Γ' can be expanded in a Taylor series about the equilibrium state, e.g. for κ':

$$\kappa' = \kappa'_{eq} + \left.\frac{\partial \kappa'}{\partial \Gamma'}\right|_{eq} (\Gamma' - \Gamma'_{eq}).$$

The surface viscosities can be incorporated in the stress balance at the interface. In so doing, a new dimensionless group appears:

$$\Phi = \frac{\kappa'_{eq} + \epsilon'_{eq}}{R'\mu'}.$$

Assuming that Φ is an $O(1)$ quantity, both the normal and tangential stress balances in the hemispherical cap region remain unchanged. In the transition region, however, the tangential stress condition, (4.5) becomes:

$$\frac{\partial v_{\zeta(0)}}{\partial \rho} = E\frac{\mathrm{d}\Gamma_{(2)}}{\mathrm{d}\zeta} - \Phi\frac{\partial^2 u_s}{\partial \zeta^2} \quad \text{at} \quad \rho = h_{(0)}(\zeta). \tag{5.2}$$

Rescaling the equations in canonical form, the incorporation of κ' in the governing equations simply modifies the definition of M to be:

$$M = \frac{E + \Phi}{K_\Gamma h_\infty}. \tag{5.3}$$

Using this definition for M, and considering the results given above, the role of surface viscosities can be understood. Interfaces with surface viscosities require larger pressure drops to aspirate the flow and leave thicker wetting layers along the capillary walls. The effects of surface viscosities are directly additive to Marangoni effects that result from small departures from surface equilibrium states. Both are bounded below by the clean interface and above by the maximum surfactant effect models.

REFERENCES

AGRAWAL, M. L. & NEUMAN, R. 1988 Surface diffusion in monomolecular films II. Experiment and theory. *J. Colloid Interface Sci.* **12**, 366–380.

BARTHÈS-BIESEL, D., MOULAI-MOSTEFA, N. & MEISTER, E. 1986 Effect of surfactants on the flow of large gas bubbles in capillary tubes. *Proc. Physicochem. Hydrodyn. NATO Conf.* La Rabida, Spain (ed. M. Verlarde).

BORHAN, A. & MAO, C.-F. 1992 Effect of surfactants on the motion of drops through circular tubes. *Phys. Fluids* A **4** (12), 2628–2640.

BRETHERTON, F. P. 1961 The motion of long bubbles in tubes. *J. Fluid Mech.* **10**, 166–168.

CHANG, H. C. & RATULOWSKI, J. 1987 Bubble transport in capillaries *AIChE Annual Meeting*, 15–20 November, New York, paper 681.

CHEN, J. D. 1985 Measuring the film thickness surrounding a bubble inside a capillary. *J. Colloid Interface Sci.* **109**, 341–349.

DJABBARAH, N. F. & WASAN, D. T. 1982 Dilatational viscoelastic properties of fluid interfaces – III. *Chem. Engng Sci.* **37** (2), 175–184.

GINLEY, G. M. & RADKE, C. J. 1989 The influence of soluble surfactants on the flow of long bubbles through a cylindrical capillary. *ACS Symp. Series*, **396**, 480–501.

GOLDSMITH, H. L. & MASON, S. G. 1963 The flow of suspensions through tubes II. Single larger bubbles. *J. Colloid Interface Sci.* **18**, 237–261.

HERBOLZHEIMER, E. 1987 The effect of surfactant on the motion of a bubble in a capillary *AIChE Annual Meeting*, 15–20 November, New York, paper 68.

HIRASAKI, G. & LAWSON, J. B. 1986 Mechanism of foam flow in porous media: apparent viscosity in smooth capillaries. *Soc. Petr. Engng J.* **25**, 176–190.

JIANG, T.-T., CHEN, J.-D. & SLATTERY, J. C. 1983 Nonlinear interfacial stress-deformation behavior measured with several interfacial viscometers. *J. Colloid Interface Sci.* **96**, 7–19.

LEVICH, V. G. 1962 *Physicochemical Hydrodynamics*. Prentice Hall.

MARCHESSAULT, R. F. & MASON, S. G. 1960 Flow of entrapped bubbles through a capillary. *Ind. Engng Chem.* **52** (1), 79–81.

PARK, C. W. 1991 Effects of insoluble surfactants on dip coating. *J. Colloid Interface Sci.* **146**, 382–394.

PARK, C. W. 1992 Influence of soluble surfactants on the motion of a finite bubble in a capillary tube. *Phys. Fluids* A **4** (11), 2335–2346.

PARK, C. W. & HOMSY, G. M. 1983 Two phase displacement in Hele-Shaw cells: Theory. *J. Fluid Mech.* **139**, 291–308.

RATULOWSKI, J. & CHANG, H. C. 1990 Marangoni effects of trace impurities on the motion of long gas bubbles in capillaries. *J. Fluid Mech.* **210**, 303–328.

SCHWARTZ, L. W., PRINCEN, H. M. & KISS, A. D. 1986 On the motion of bubbles in capillary tubes. *J. Fluid Mech.* **172**, 259–275.

SCRIVEN, L. E. 1960 Dynamics of a fluid interface equation of motion for Newtonian surface fluids. *Chem. Engng Sci.* **12**, 98–108.

STEBE, K. S., LIN, S. Y. & MALDARELLI, C. 1991 Remobilizing surfactant retarded particle interfaces. I. Stress-free conditions at the interfaces of micellar solutions of surfactants with fast sorption kinetics. *Phys. Fluids* A **3** (1), 3–20.

WEI, L. Y. & SLATTERY, J. C. 1976 Experimental study of nonlinear surface stress-deformation behavior with a deep channel viscometer. *Colloid and Interface Science*, vol. 4, pp. 399–420. Academic.